Rapid Response of the Norwegian Atlantic Slope Current to Wind Forcing

NICOLA JANE BROWN,[a,b] CECILIE MAURITZEN,[b] CAMILLE LI,[c,d] ERICA MADONNA,[c,d] PÅL ERIK ISACHSEN,[a,b] AND J. H. LACASCE[a]

[a] *Department of Geosciences, University of Oslo, Oslo, Norway*
[b] *Division for Ocean and Ice, Norwegian Meteorological Institute, Oslo, Norway*
[c] *Geophysical Institute, University of Bergen, Bergen, Norway*
[d] *Bjerknes Centre for Climate Research, Bergen, Norway*

(Manuscript received 25 January 2022, in final form 22 September 2022)

ABSTRACT: We explore drivers of variability in the Norwegian Atlantic Slope Current, which carries relatively warm Atlantic Water toward the Barents Sea and Arctic Ocean, using Copernicus Marine Environment Monitoring Service (CMEMS) satellite altimetry data and TOPAZ4 ocean reanalysis data. Previous studies have pointed to a variety of causes, on a variety of time scales. We use data with daily resolution to investigate day-to-day changes in ocean transport across three sections crossing the shelf-slope of Norway (Svinøy, Gimsøy, and the Barents Sea Opening). The highest (lowest) extremes in transport at all sections develop over two days as a cyclonic (anticyclonic) atmospheric pressure system approaches from the southwest, piling up (extracting) water at the coast of Norway. The actual peak is reached when the pressure system passes the site of measurement, and the transport then relaxes for the next two days as the system continues northward along the coast. Other sources of short-term variability, such as propagating continental shelf waves and baroclinic instability, are unlikely to yield covariability over large separations. Monthly variability in the current can also be explained by passing weather systems since their numbers and intensity vary greatly from month to month. Many studies of longer-term variability, especially in the Barents Sea Opening, have pointed to the North Atlantic Oscillation (NAO) as the main cause of variability. Our results show that passing weather systems offer a better explanation of month-to-month variability.

KEYWORDS: Arctic; Atmosphere-ocean interaction; Currents; Ocean circulation; Subseasonal variability

1. Introduction

The northernmost limb of the Atlantic meridional overturning circulation enters the Nordic seas as the Norwegian Atlantic Current (NwAC). Hydrographically, Atlantic Water appears as a broad slab of warm and salty water (Fig. 1a), but the current is intensified in two narrow branches, one following the shelf edge through the Faroe–Shetland Channel and along the Norwegian shelf, and the other farther west at the front between the Atlantic Water and the colder Polar Water (Orvik and Niiler 2002; see also Figs. 1a and 1b). The Norwegian Atlantic Current retains its two-branch structure through the Nordic seas with one branch, known as the Norwegian Atlantic Slope Current (NwASC), centered over the 700-m isobath and with the outer branch following the 2000-m isobath to the west (Poulain et al. 1996; Orvik and Niiler 2002). At the Barents Sea Opening (BSO) there is a bifurcation of the NwASC, with part of the current entering the relatively shallow Barents Sea and the remainder continuing north toward Fram Strait as the West Spitsbergen Current (WSC).

The Norwegian Atlantic Current, particularly the slope current, has been monitored since the 1990s at Svinøy, Gimsøy, and the BSO (see Fig. 1b) by the Norwegian Institute of Marine Research (IMR). Even before the era of the current meter moorings, the IMR ran standard hydrographic ship lines along the sections, such that the hydrographic time series go back to the 1950s. The current meter data (e.g., at Svinøy) exhibit large variability at all time scales from hourly to interannual, including a strong seasonal signal (Orvik and Skagseth 2003b; Orvik 2022). Using these observational records as well as model hindcasts, there have been numerous studies to estimate the strength of the current and to identify the causes of its variability in this region. Various potential drivers of variability have been proposed, but uncertainty remains about which are the most important at different time scales.

The inspiration for some studies has been papers on continental shelf waves (e.g., Adams and Buchwald 1969; Gill and Schumann 1974; Allen 1975; Brink 1991). These are coastally trapped waves that exist due to the dynamical effect of a sloping bottom. In a study of current variability over the Scottish shelf, Gordon and Huthnance (1987) identified two modes of the response to wind forcing during winter storms: a "quasi-steady" and an oscillating one. The former represents a steady balance between Coriolis acceleration of the along-isobath flow and the pressure gradient arising from Ekman-induced pile-up on the shelf, while the oscillating portion was identified as a shelf wave. Applying this concept to the Norwegian shelf, Skagseth and Orvik (2002) employed empirical orthogonal function (EOF) analysis on roughly one year of current meter data from the Svinøy region. The first (cross slope) EOF was linked to the directly forced quasi-steady component. This was coherent with the local wind forcing, with a lag of 12 h. The second and third EOFs, with time scales of several days to a week, were hypothesized to be shelf wave modes. In a subsequent study (Orvik and Skagseth 2003a),

Corresponding author: N. J. Brown, nicolajb@met.no

DOI: 10.1175/JPO-D-22-0014.1

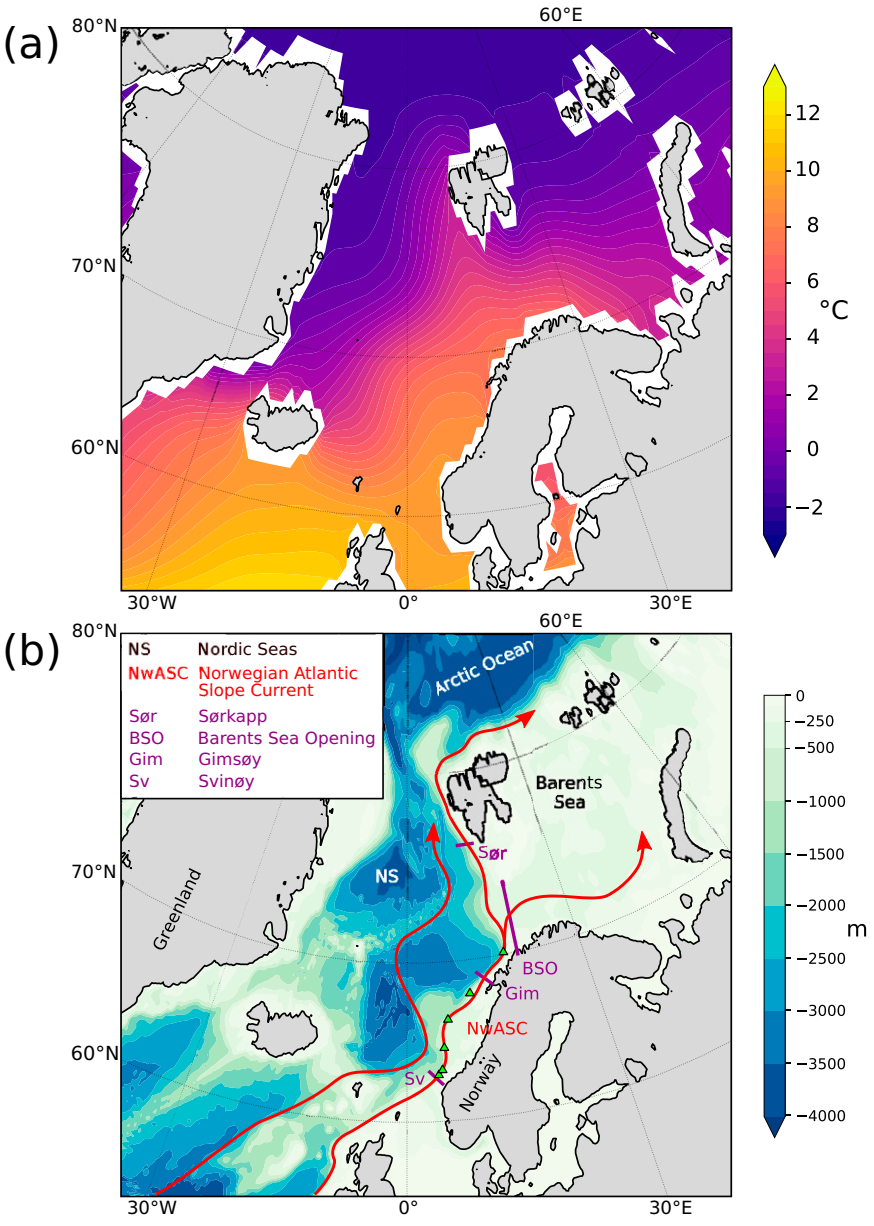

FIG. 1. (a) Sea surface temperature in the Nordic and Barents Seas from the Polar Science Center Hydrographic Climatology. (b) Location of the study area. Colored shading indicates bathymetry from the TerrainBase 1/12° Global Terrain Model. The red lines show the main flows of Atlantic Water through the Nordic seas. The purple lines show the positions of the transects along which flows are integrated in this study. The green triangles show the locations for which across-slope velocities are calculated.

the authors suggested that the shelf waves were excited by changes in the wind stress curl in the subpolar gyre, at 55°N, occurring 15 months previously. The wind stress curl in the North Atlantic was theorized to excite a baroclinic Rossby wave, which was then converted to a barotropic shelf wave on entering the Nordic seas.

Other studies support the importance of direct wind forcing. Analyzing a 4-yr-long current meter time series from the Barents Sea Opening, Ingvaldsen et al. (2004) deduced that changes in the velocity field are generated by the local wind field through Ekman transport on daily time scales. Skagseth (2004), from an EOF analysis of TOPEX/ERS satellite altimeter data along the entire Norwegian slope as well as seven years of current meter data from Svinøy, found that the seasonal response was correlated with the large-scale winds. Richter et al. (2009) found a strong link

between the passage of cyclones through the Nordic seas and the variability of Atlantic inflow to the Nordic seas, as estimated from current meters positioned in the main inflow branches and in the NwASC at Svinøy. They showed that enhanced flow along the Norwegian coast was associated with strengthened along-slope winds and positive sea level anomalies on the shelf, supporting the hypothesis that Ekman pile-up along the coastal boundary causes an increased sea level gradient, which leads to a strengthening in the geostrophic current. Analysis by Richter et al. (2012) using satellite and tide gauge data supported this conclusion. Further north, Lien et al. (2013) investigated short-term variability in the two main branches of Atlantic Water inflow to the Arctic Ocean—the WSC through the Fram Strait and the Barents Sea inflow—using an ocean model as well as current meter observations from the northern BSO slope. They attributed variability in the relative strengths of the two branches to periods of Ekman forcing around the northern Barents Sea region, which leads to a decrease in sea surface height over the northern Barents Sea shelf, resulting in turn in a cyclonic circulation anomaly along the slope around the northern Barents Sea shelf area.

A further potential source of variability in the Norwegian Atlantic Current arises from the internal instability of the current itself. There is a broad region of warm water between the two velocity cores. The exchange between the cores is likely mediated by baroclinic instability of the cores, giving rise to lateral heat fluxes (Isachsen et al. 2012; Trodahl and Isachsen 2018). The deformation scale (10–15 km) eddies resulting from the instability also likely lead to current fluctuations over the slope.

To summarize, variability in the Norwegian Atlantic Current has been studied on a variety of time scales. In this study we focus only on short (daily) time scales, and even so there are several potential mechanisms proposed in the literature. These include 1) shelf waves, forced by remote winds; 2) the "direct" response to local Ekman forcing; and 3) mesoscale eddies, generated by baroclinic instability.

Examining the variability using datasets that resolve the daily time scales of currents, sea surface height, and atmospheric forcing fields, we will be able to directly resolve the dynamical mechanisms at play. We will also show that the results have implications for how to interpret lower-frequency variability.

2. Data and methods

In this study we have used two products from the Copernicus Marine Environment Monitoring Service (CMEMS), namely the SSALTO/DUACS delayed-time multisatellite product (Pujol et al. 2016, 2018) and the TOPAZ4 ocean reanalysis product (Sakov et al. 2012). In addition, we have used the ERA-Interim atmospheric reanalysis product from the European Centre for Medium-Range Weather Forecasts (ECMWF) (Dee et al. 2011).

a. Satellite altimetry data

We have used sea level anomalies (SLAs; i.e., the difference between the time-varying, altimetry-derived sea surface height and the long-term mean height) from the SSALTO/DUACS dataset for the period from 1 January 1993 to 31 December 2018. These are provided at 1/4° horizontal resolution and daily temporal resolution. We have also used surface geostrophic velocities from the same dataset. These are calculated from gradients in sea surface height η using the relations

$$u = -\frac{g}{f}\frac{\partial \eta}{\partial y} \quad \text{and} \quad v = \frac{g}{f}\frac{\partial \eta}{\partial x},$$

where u and v are surface geostrophic velocities in the x (zonal) and y (meridional) directions respectively, g is acceleration due to gravity, and f is the Coriolis parameter.

The multisatellite product incorporates data from all available altimeters at any time to maximize signal sampling to best reproduce mesoscale ocean features but is not homogeneous in time because the combination of altimeters used varies. This is in contrast to a two-satellite product that prioritizes homogeneity, which is important for some operational applications. Corrections are applied to the altimeter data to account for instrument and measurement errors; errors due to the effect of dry gases and water vapor (dry and wet troposphere corrections) and ions (ionospheric corrections) in the atmosphere and the effect of the sea surface state on reflection of the altimeter signal, as well as ocean tides, the inverse barometer effect, and wind field (dynamical atmosphere corrections). Although this is a global dataset, it has been evaluated for our region and shown to be in good agreement with tide gauge measurements and drifter trajectories in the Nordic seas and ice-free parts of the Barents Sea (Volkov and Pujol 2012).

In addition, we show mean dynamic topography (MDT) from the CNES-CLS18 product (Mulet et al. 2021), also available from CMEMS, with a horizontal resolution of 1/8°. This is an estimate of the mean height of the sea surface above the geoid in the period 1993–2012, and reflects the long-term mean ocean circulation. It is derived from satellite gravimetry and altimetry data and in situ drifter and hydrographic observations.

b. Ocean reanalysis data

Daily mean SSH and full-depth ocean velocities for the period 1 January 1991–31 December 2018 were taken from the TOPAZ4 ocean reanalysis system (Sakov et al. 2012). The system uses the Hybrid Coordinate Ocean Model (HYCOM), with a horizontal resolution of 12–16 km, coupled to a sea ice model and an ensemble Kalman filter for the weekly assimilation of remotely sensed sea level anomalies, sea surface temperature, and sea ice concentration and thickness, as well as in situ temperature and salinity measurements. Volume transports from the reanalysis have been validated with independent observations (i.e., observations that have not been assimilated into the model) from Svinøy and the BSO by Sakov et al. (2012). We have also compared volume transports with observations

from a current meter at Svinøy[1] and found that the TOPAZ transports are at least as closely correlated with the observed current as are estimates of the current derived from the observation-based CMEMS satellite altimetry product (see section 2d). The reanalysis has been found to perform well across the wider Arctic region, including the Nordic seas, especially with respect to near-surface variables (Xie et al. 2017).

c. *Atmospheric reanalysis data*

Sea level pressure and surface wind stress were taken from the 1° × 1° resolution ERA-Interim reanalysis (Dee et al. 2011). Daily means were calculated from the 6-hourly values provided.

d. *Velocity and transport calculations*

An underlying driver for the current work has been to use satellite altimetry data to diagnose ocean velocities. Some studies have shown that relative to subsurface data (such as from Argo floats, which typically drift with ocean currents at a depth of 1000 m; https://argo.ucsd.edu/), assimilation of altimetric data is particularly important for the large-scale circulation (see, e.g., Oke et al. 2015). However, other studies (e.g., Skagseth 2004) have shown that gradients of sea surface height calculated from satellite altimetry data can be a good indication of the variability in narrow currents such as the NwASC. In this study we have used estimates of ocean current velocities from satellite altimetry, ranging from the most direct estimate (geostrophic velocities based on surface slope) to those calculated using a fully three-dimensional ocean reanalysis product (where satellite altimetry data are assimilated along with a slew of other data products).

We have calculated proxies for transport across four transects covering the main pathways of Atlantic Water in the NwASC and WSC: at Svinøy (62.466°N, 5.000°E–63.266°N, 3.250°E), Gimsøy (68.400°N, 14.000°E–69.176°N, 11.750°E), the Barents Sea Opening (BSO) (69.875°N, 19.125°E–74.125°N, 19.125°E), and Sørkapp (76.375°N ,11.125°E–76.375°N, 14.375°E), each marked in purple in Fig. 1b. These transects occupy similar positions to the standard sections for which time series of hydrographic measurements are maintained by the Institute of Marine Research (IMR) (https://www.hi.no/hi/forskning/marine-data-forskningsdata). From the altimetry data we integrated the across-transect component of the surface geostrophic velocities along the transects, interpolating the velocities onto equidistant points along the transects in the case of Svinøy and Gimsøy, which do not lie along the data grid. For the ocean reanalysis product we took the difference between the daily mean sea surface heights at the coastal and offshore ends of each transect (see section 2a). In each case, we used the values for the nearest grid point. In addition, we calculated the top-to-bottom volume transports across the transects from the full depth reanalysis velocities. The current is not entirely barotropic along the length of the shelf—indeed, Fer et al. (2020) found strong variation with depth in current meter observations at Gimsøy—and so the full depth integration includes some weak recirculating flow at depth, but in this study we focus on the high-frequency (daily) variability of the current and over these time scales we expect adjustment to be barotropic.

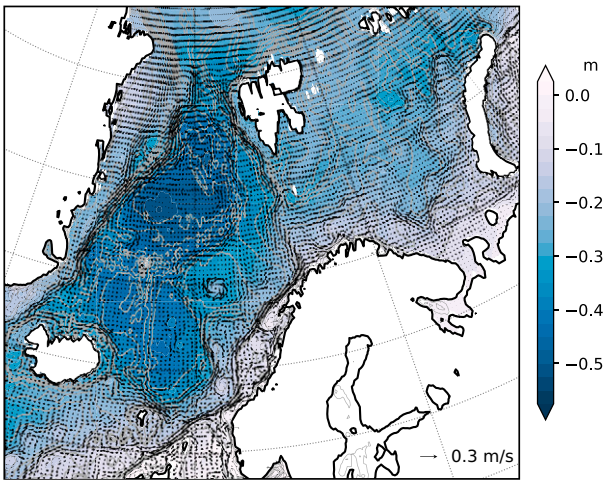

FIG. 2. Mean dynamic topography (shading) and long-term mean surface geostrophic currents (arrows) from altimetry and in situ observations, averaged over the period 1993–2012. The gray contours indicate bathymetry.

To test for the presence of continental shelf waves in the TOPAZ4 reanalysis, we compared estimates of across-slope velocities at depth at a series of locations along the continental slope (shown by the green triangles in Fig. 1b). The water depth at each of these locations is 830 ± 20 m, and so the locations are effectively aligned along a bathymetric contour. Components of velocity normal to the tangent to the contour at each location were calculated for a depth of 763 m (a standard depth level for the dataset chosen to be clear of the bottom boundary layer but still deep within the water column). At this depth, velocities should be representative of the barotropic flow field and remote from the influence of the surface and bottom boundary layers.

3. Results

a. *The long-term mean ocean state*

The long-term MDT and mean surface geostrophic currents, as observed in the CMEMS altimetry data, are shown in Fig. 2. The darker blue shades in the deeper Nordic basin

[1] Orvik and Skagseth (2003b) found that the volume flux as calculated from an array of current meters at Svinøy could be estimated from velocities measured with a single current meter in the core of the current. We have compared velocities from a current meter in this same location with TOPAZ volume transports, each smoothed by applying a 7-day low-pass filter for sample 1-yr periods (2013, 2014, and 2015), and found correlation coefficients of 0.62, 0.74, and 0.72, respectively. These are slightly higher than the correlations between the measured currents and estimates of the current from satellite altimetry for the same periods (0.46, 0.62, and 0.71), and only slightly lower than the correlation given by Orvik and Skagseth (2003b) between the velocities from the single meter and transports calculated from the whole array for their test year (0.80).

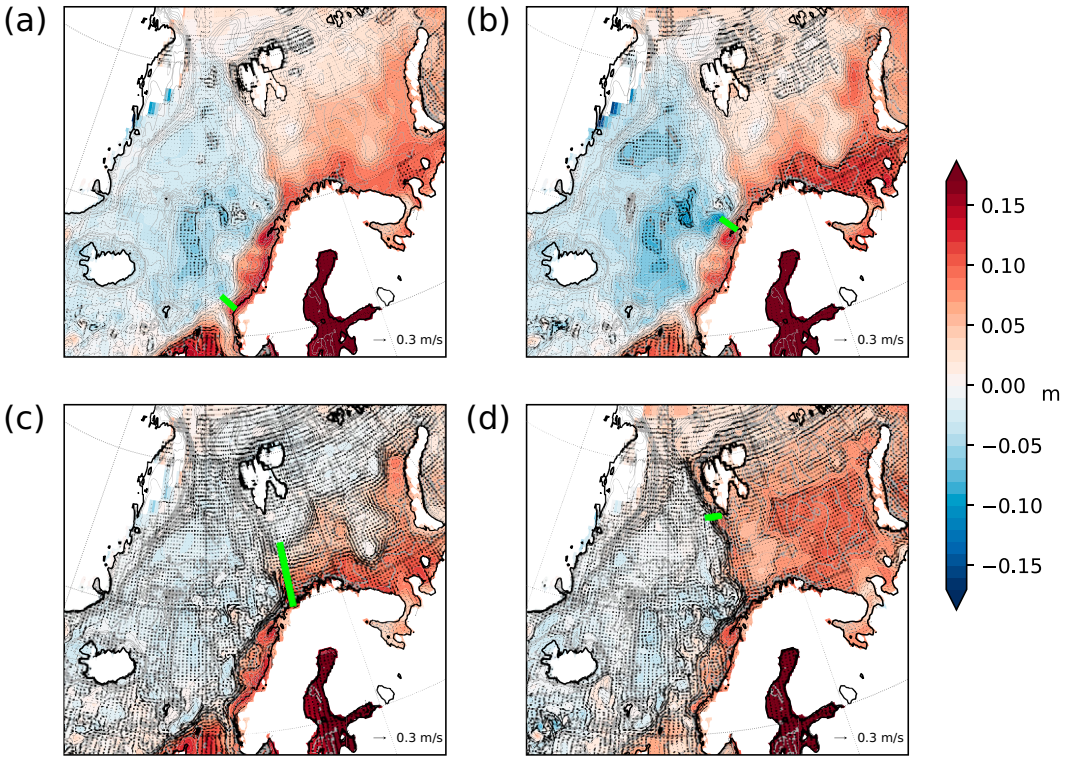

FIG. 3. (a) CMEMS sea level anomalies (SLAs) and anomalies in surface geostrophic currents averaged over days of high flow at Svinøy (green line; see text for details). (b)–(d) As in (a), but for days of high flow at Gimsøy, BSO, and Sørkapp respectively.

indicate lower dynamic topography associated with cyclonic flow around the basin. A marked gradient in dynamic topography and stronger velocities are apparent along the Norwegian shelf break. This is the topographic steering discussed by Poulain et al. (1996) and Orvik and Niiler (2002) (see Fig. 1). Closer examination shows that the currents follow bottom topography (gray contours and Fig. 1) closely along the shelf, passing Spitsbergen, and also through the Barents Sea Opening into the Barents Sea. The strong topographic steering, even of time-mean surface currents, is a result of topography dominating the ambient potential vorticity (PV) gradients at these high latitudes (Isachsen et al. 2003; Nøst and Isachsen 2003; Timmermans and Marshall 2020).

b. *Sea level and surface geostrophic velocities associated with high flow*

To investigate possible mechanisms driving variability in the NwASC we consider the characteristic anomalies from the long-term mean state during periods when flow at the selected locations along the path of the current is particularly high. Figures 3a–d are composites of CMEMS SLA and surface geostrophic velocity anomalies averaged over all days for which integrated surface velocities at each of the transects—Svinøy, Gimsøy, BSO, and Sørkapp respectively—exceeded the 98th percentile. The green lines show the locations of the transects.

Days of high flow at Svinøy and Gimsøy (Figs. 3a,b) are marked by a slightly negative anomaly from the long-term mean (i.e., a lower than average sea level) within the deep basin and positive anomalies (higher sea levels) on the shelves to the north of the British Isles and along the Norwegian coast. As with the MDT, the steepest gradient in anomaly is seen along the shelf, perpendicular to the mean flow. The resulting increase in flow, like the time mean current, follows the bathymetry closely. For days of extreme high flow at BSO (Fig. 3c), higher than average sea levels are again seen along the Norwegian shelf, but the gradient in sea level anomaly across the Barents Sea Opening is more marked than it is for those days when flow is high at Svinøy, farther to the south. In contrast, when flow is high at Sørkapp (Fig. 3d), SLAs are positive across the entire Barents Sea, such that the gradient in SLA is most marked along the entrance to the Barents Sea. This is associated with a strengthening in surface geostrophic velocities in the West Spitsbergen Current.

c. *3D velocity field versus surface geostrophic velocities*

The patterns of sea level anomaly associated with enhanced flow at each of the transects are consistent with the piling up of water along the Norwegian coast by Ekman transport, in a similar manner to the mechanism described by Gordon and Huthnance (1987) for their directly forced "quasi-steady" component (i.e., not the wave component). Ekman transport develops on inertial time scales, which is faster than the effective temporal resolution of the altimetry data. (Despite interpolation onto a daily dataset, the actual passing of the satellites

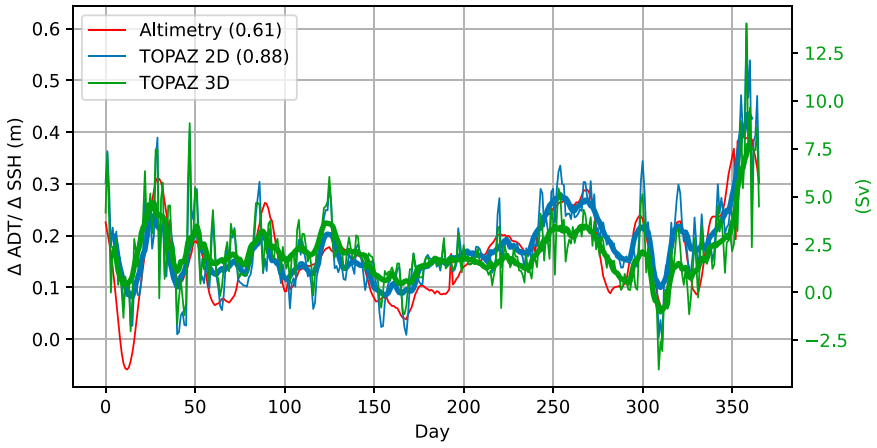

FIG. 4. Shown in red (left axis) is the difference in absolute dynamic topography (ADT) from CMEMS altimetry along the Svinøy transect for the year 2016. In blue (left axis) is the difference in SSH from TOPAZ4 reanalysis along the same transect. In green (right axis) are volumetric transports calculated from full-depth ocean velocities, also from TOPAZ4. Thin lines represent daily data and thick lines indicate the 10-day running mean. The values in parentheses in the legend are correlation coefficients between the CMEMS and TOPAZ volumetric transport time series, and between the TOPAZ SSH difference and volumetric transports.

occurs at a lower frequency.) Therefore we have repeated the investigation of extreme flows at each of the transects using TOPAZ4 sea surface heights, which have true daily resolution.

A comparison of the proxies for flow across the Svinøy transect (see section 2d) over an illustrative year, 2016, appears in Fig. 4. The red line for the altimetry shows the difference along the transect of absolute dynamic topography (ADT = SLA + MDT); that is, it includes the long-term mean state to allow easier comparison with the difference in SSH from the TOPAZ reanalysis (in blue). (Note that both ADT and SSH represent the height of the sea surface: the former is measured relative to the geoid while the datum for the latter is the reference ellipsoid, but the distinction is irrelevant for our study of the time variation in the current.) The thinner blue line represents daily TOPAZ values, while the thicker blue line shows a 10-day running mean. There is high variability, even over daily time scales, in the TOPAZ time series, confirming the utility of its higher temporal resolution in investigating the short-term behavior of the ocean. Correspondence between the two in terms of variability is quite good at weekly to monthly time scales (correlation coefficient 0.73). This is unsurprising, given that the same altimetry data are assimilated in the TOPAZ4 system, and gives us confidence to proceed with analysis using the TOPAZ data.

Also shown in Fig. 4, in green, is the full-depth integration of volumetric flux across the Svinøy transect calculated from three-dimensional currents from the TOPAZ4 reanalysis. There is again a good match (with correlation coefficient 0.88) between variability in sea surface gradient and variability in full-depth transports in TOPAZ, confirming the validity of the use of TOPAZ sea surface heights as a proxy for short term current variability. As mentioned above, we would expect the fast (daily to weekly time scale) current fluctuations to be essentially barotropic, and this result confirms that hypothesis.

In the rest of this study we will, rather than using the sea level altimetric data directly, use the TOPAZ ocean reanalysis data, giving us not just daily resolution but also the added benefit of a fully consistent, three-dimensional dynamical system for our analysis.

d. Day-by-day development of high velocity events

To gain insight into the behavior of the ocean in the lead-up to periods of high and low flow, with the aim of identifying the main forcing mechanisms, we have identified those high and low flow days representing the commencement of each extreme event (the day 0). Here, we select only those dates for each event on which flow at each transect *first* fell within the highest or lowest two percentiles, and exclude all high and low flow days that fall within seven days of a previous high or low flow day respectively. Our intention is to understand how the ocean moves from a state of moderate flow to a state of extreme flow, to better elucidate the drivers of extreme flow. The characteristic SLA and atmospheric forcing [represented by sea level pressure (SLP) anomalies] for extreme flow events are examined via lagged daily composites.

Figure 5 shows composites of SLA and SLP for the buildup to extreme high flow at Svinøy, from day −2 until day +2. On day 0, the first day falling within the extreme category (Fig. 5f), the sea level is anomalously depressed in the interior of the Norwegian Sea and elevated on the shelf. There is a deep atmospheric low pressure system located directly offshore the Svinøy section (Fig. 5c). Going back one day (to Figs. 5b,e) the low pressure is centered farther southwest (over Iceland), whereas two days earlier (Figs. 5a,d) one can barely identify a SLP anomaly in the Norwegian Sea. In Fig. 5k is shown the anomaly in volume transport for each day in Fig. 5. Absolute transport more than doubles from day −2 to day 0. The transport does not relax as fast: Fig. 5k shows that at days +2 and +3 the

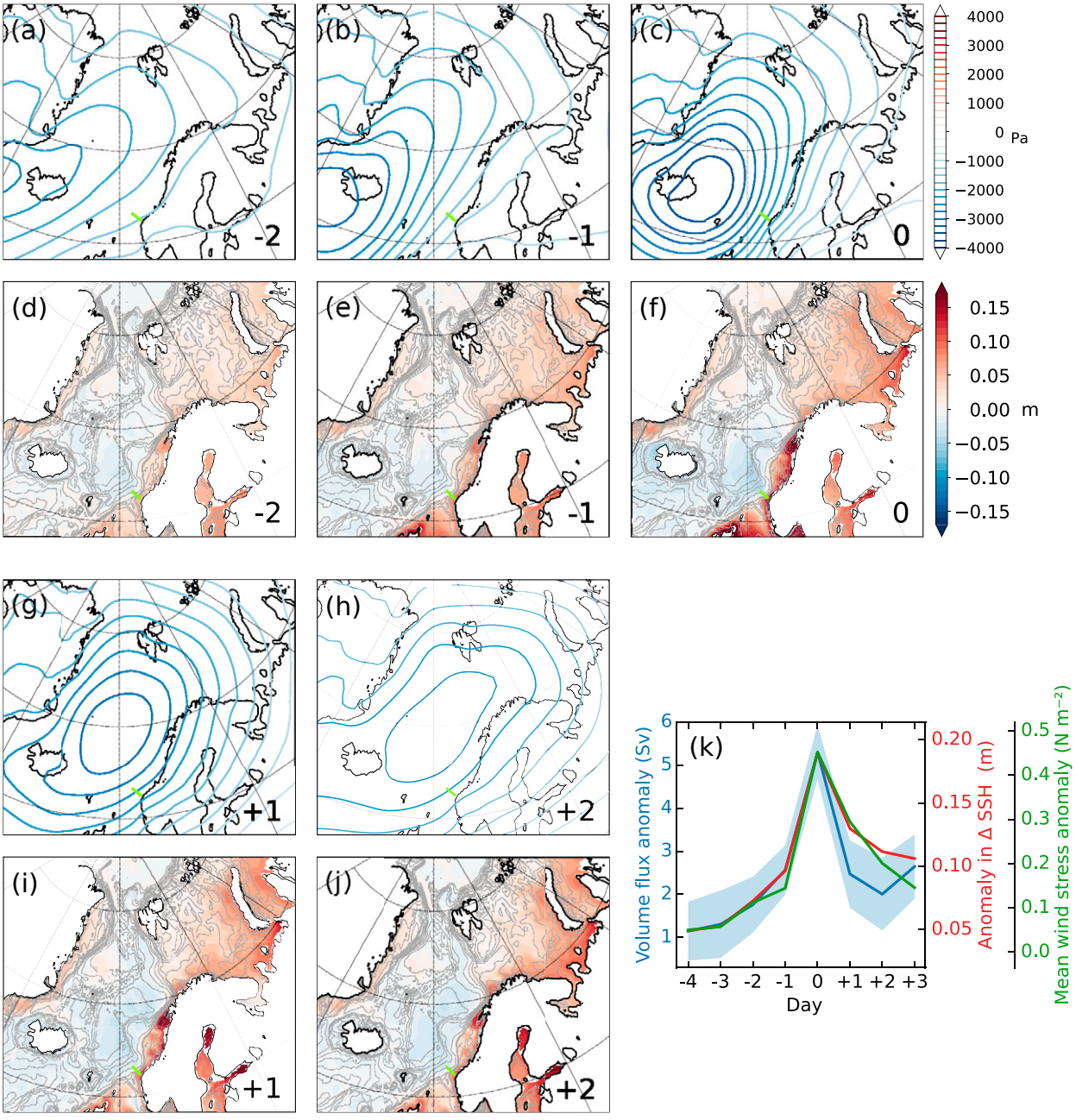

FIG. 5. (a) Mean anomalies in SLP from ERA-Interim for all dates two days before the first day of each high flow event at Svinøy (day −2). (b),(c),(g),(h) As in (a), but for days −1, 0, +1, and +2, respectively. (d)–(f),(i),(j) Mean anomalies in TOPAZ SSH for the same groups of days. (k) Mean anomalies in volumetric transport (blue), SSH difference (red), and along-slope wind stress (green) at Svinøy for all dates from four days before to three days after the first days of extreme flow events. The blue shading indicates standard error (±1 standard deviation divided by $\sqrt{N}$) in volumetric transport for days included in the composite.

transport is still elevated compared to the onset of the event. Past the peak, the low pressure system moves northeastward (Figs. 5g,h) and subsides in intensity.

Figure 5 suggests that the highest-velocity events at Svinøy are directly forced by passing low pressure systems (cyclones), which cause divergence of water under the center of the cyclones and Ekman transport toward the shelf with corresponding elevated sea level there. Anomalies in sea level elevation and the wind stress at Svinøy are displayed in Fig. 5k with the volume transport. In practice, the Ekman transport that causes coastal pile-up operates over a larger area than the transect itself, but this measure gives an indication of wind stress in the locality of the transect. The correspondence between evolution of local atmospheric forcing and ocean response is striking: it is

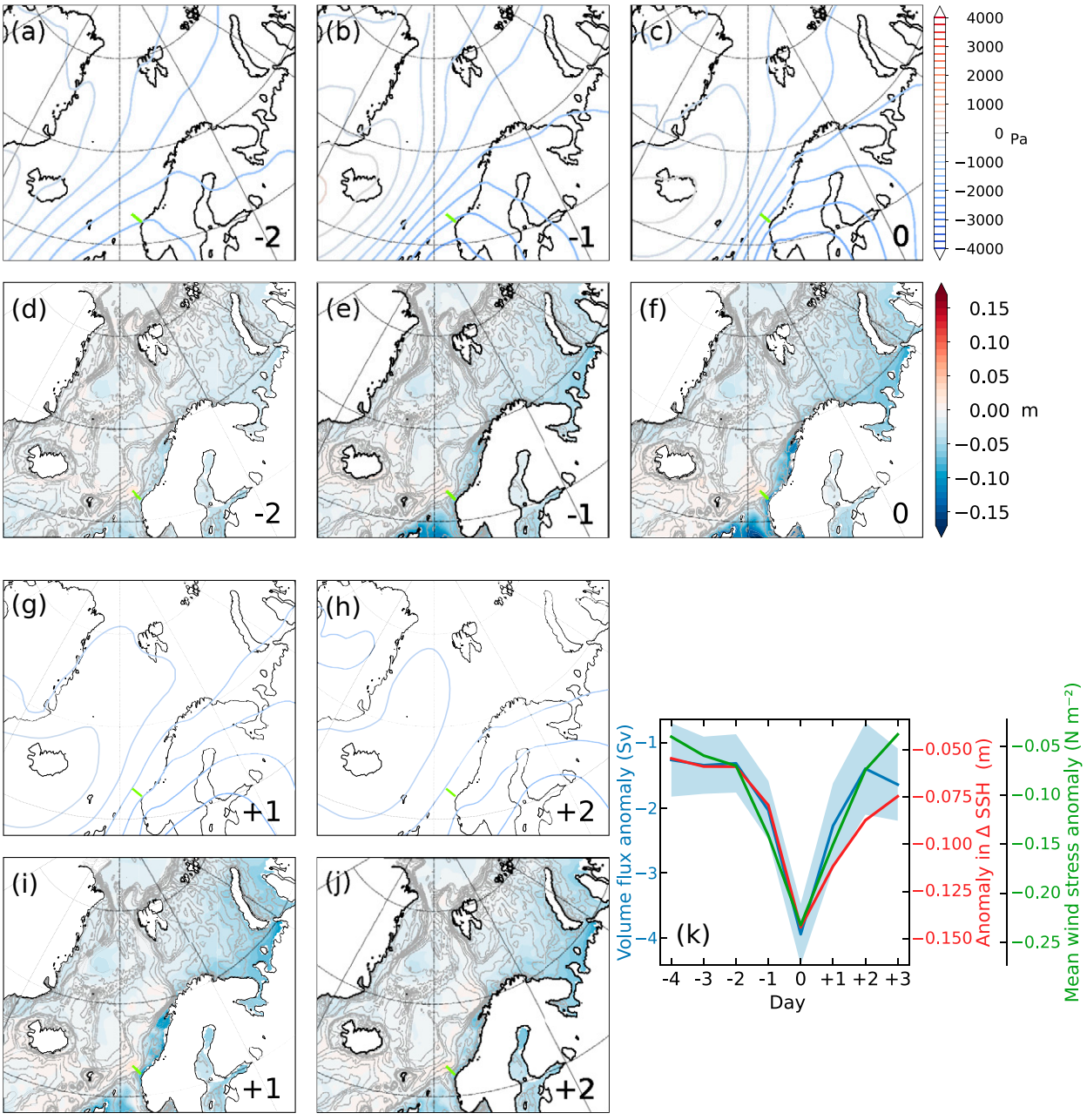

FIG. 6. As Fig. 5, but for low flow events at Svinøy.

remarkable that the ocean current responds to the winds so fast, within a day.

In Fig. 6 we show the opposite situation: the day-by-day development of incidences of particularly low volume transport at Svinøy. These events are forced by anticyclones passing through the Nordic seas. Anticyclones are by nature less energetic than cyclones (Thorpe 1986; Hakim et al. 2002), so the change in sea level gradient is much less than in the high-peak event (little more than half as big when the changes from day −2 to day 0 in Figs. 5k and 6k are compared). But the direct forcing by passing atmospheric systems is in both cases as fast and as clear.

At Gimsøy (shown in Fig. 7) and the BSO (Fig. 8), extreme events are characterized by elevated sea levels along the more northern sections of the Norwegian coast and southern and eastern Barents Sea respectively. They are associated with low pressure systems centered farther north than those causing high flows at Svinøy, which points again to the importance of wind forcing in the locality for the ocean response over these short time scales. However, the volumetric flux at Gimsøy appears to peak a day later than the wind forcing and surface velocities, and to fall off again more slowly. We do not have a dynamical explanation for a baroclinic response over these short time scales. The apparently

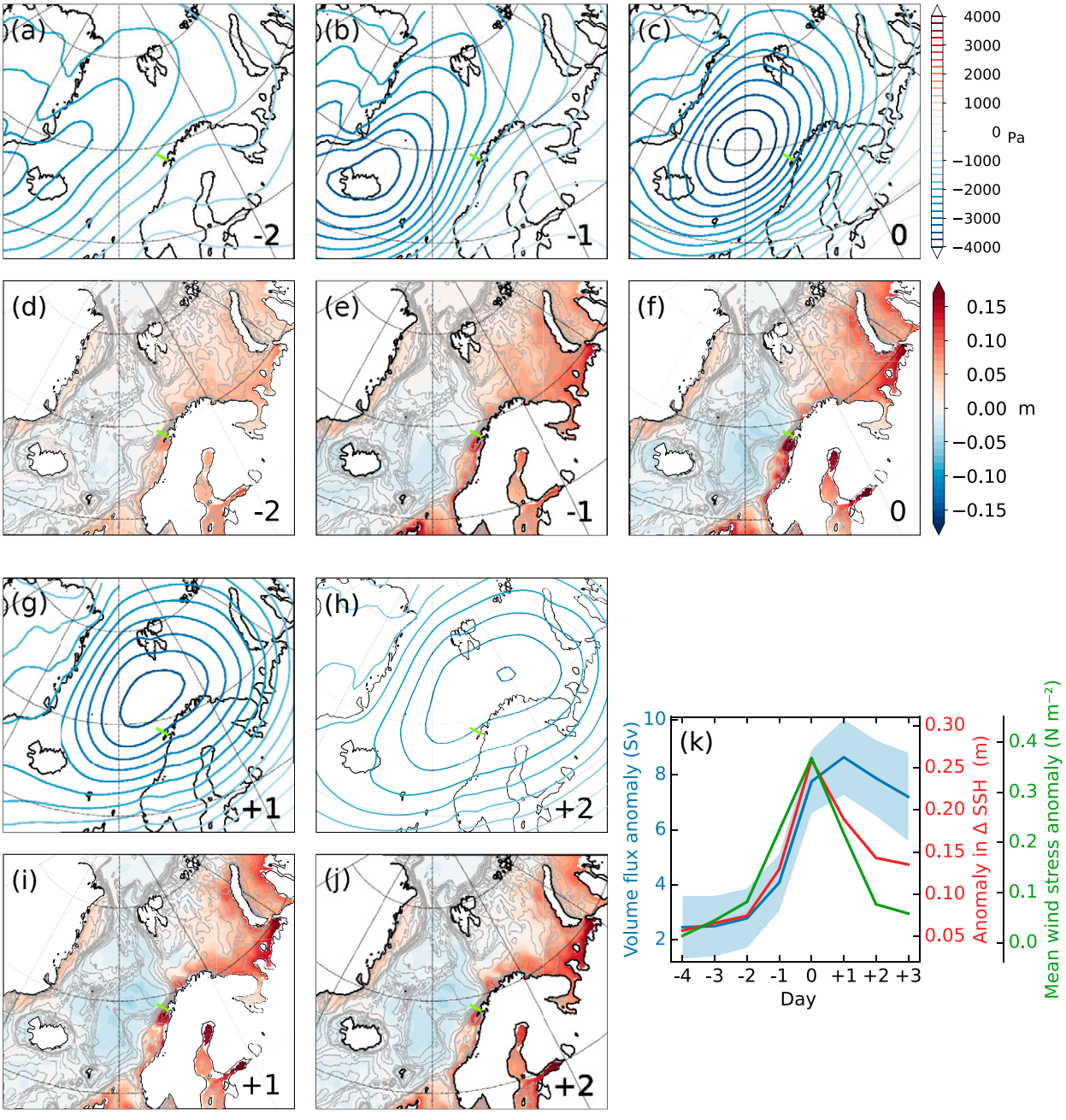

FIG. 7. As Fig. 5, but for high flow events at Gimsøy.

different behavior might be associated with the high level of instability in the current at Gimsøy compared to other locations up the Norwegian coast (Fer et al. 2020) because the shelf is narrow here and the slope steep. But the narrow, unstable current and short transect also result in a higher level of noise in the signal, and the apparent discrepancy is within the margins of error, so an alternative explanation is that it is not real.

Also at Sørkapp (Fig. A1 in the appendix) the transport almost doubles in the two days leading up to the high-velocity event and relaxes thereafter (although note that fewer individual events make up the composites for Sørkapp than for the other sections, and so the results here might be less robust). However, at this location the cyclones do not propagate northward past the site: instead there appears to be a more or less stationary low pressure system offshore to the southwest (Figs. A1c,g), and instead the sea level is increasing not just along the shelf of Svalbard but in the entire Barents Sea (Figs. A1d,e,f,i,j). Spitsbergen does not provide the long coast that Scandinavia does, which allows for coastal pile-up and a clean response to along-slope winds at Svinøy, Gimsøy and the BSO. At Sørkapp,

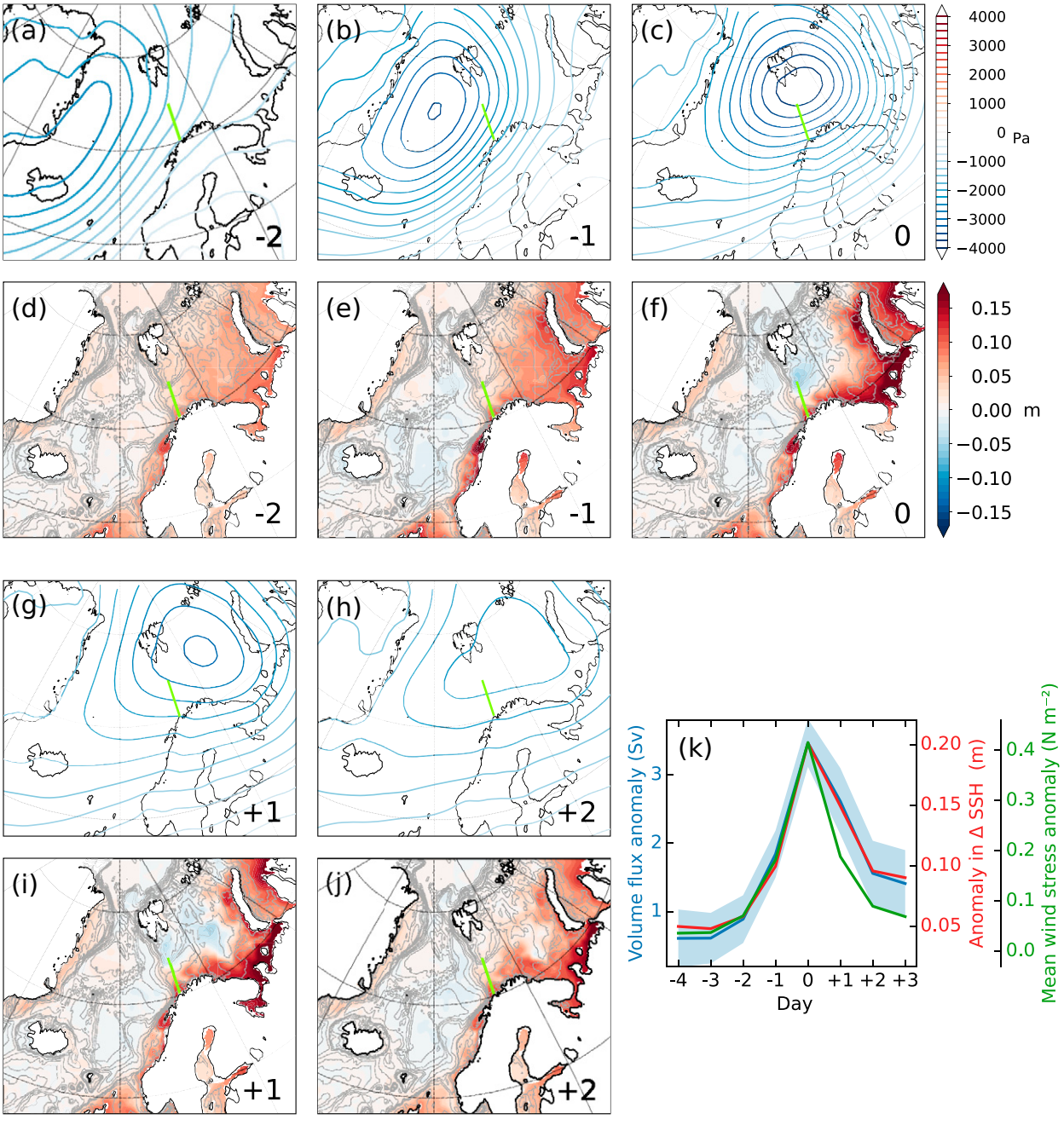

FIG. 8. As Fig. 5, but for high flow events at BSO.

the composites show anomalously low atmospheric pressure over the Nordic seas and smaller SLP anomalies over the Barents Sea.

As for Svinøy, the contrary cases (with the development of events of extremely low flow at each of the transects) appear largely opposite in pattern to the high flow events (see Figs. A2–A4 in the appendix), with higher atmospheric pressure leading to convergence of water in the central basins of the Nordic seas, lowered sea levels along the Norwegian shelf and in the Barents Sea, and reduced northward flow along the Norwegian coast.

In summary, therefore, a clear and rapid response of the ocean to local atmospheric forcing is seen in the composites for Svinøy, Gimsøy, and at the BSO. The flow response at Sørkapp is also closely tied to local winds, but the atmospheric pattern is clearly different from that at the other locations.

e. *Covariability along the path of the current*

We next examine the relationship between variability in volume fluxes at the different transects along the path of the

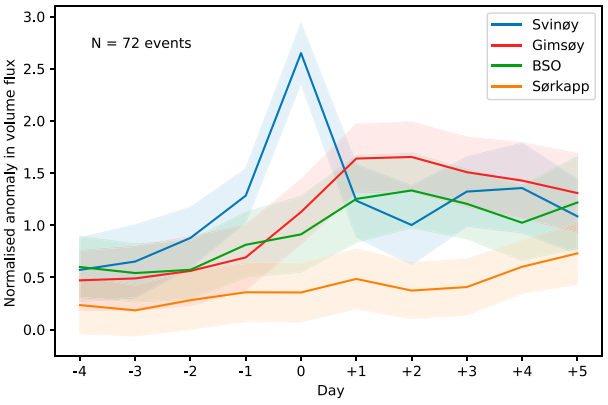

FIG. 9. Mean anomalies in volume flux across each transect, normalized by the standard deviation in flux across the transect, for all dates from four days before to five days after the first days of extreme high flow at Svinøy. The lighter shading indicates standard error.

current. There is a relatively high degree of correlation between the time series of daily mean fluxes at Svinøy and Gimsøy (Pearson correlation coefficient peaking at 0.66 at a lag of one day) and slightly less between Gimsøy and BSO (0.54 at zero lag) and between Svinøy and BSO (0.45 at a lag of two days).

The relationship is also seen in the response to forcing that generates extreme high flow. Figure 9 shows normalized anomalies in volume fluxes for the ranges of dates (slightly extended) around high flow events at Svinøy that were shown in Fig. 5k, but this time for fluxes at all transects. Peaks in flux, albeit reduced in scale, are seen at Gimsøy and at BSO a day or two after the flow peaks at Svinøy. (As before, different behavior is apparent at Sørkapp.) This could be due to a relationship between the wind forcing felt locally at each location, or it could indicate the propagation of a signal up the coast, as a shelf wave (Gordon and Huthnance 1987; Brink 1991; Skagseth and Orvik 2002; Orvik and Skagseth 2003a).

To test for the latter, we examined the covariability of the velocities at depth at locations along the continental shelf (shown by the green triangles in Fig. 1 and in more detail in Fig. 10b). To detect wave motion, we focus on the cross-isobath component of the velocity, because the along-isobath component is strongly influenced by the mean flow.

Figure 10a shows correlations between velocities at each of the locations 2–6 and at the southernmost location 1, close to the Svinøy transect. For station 2, 49 km away from station 1, there is a peak in correlation of 0.67 at a lag of one day. But by station 3 (at a direct distance of 184 km, but a little farther as measured along the shelf) peak correlation has fallen to 0.19, at a lag of three days. For station 4 (at a direct distance of 370 km) the peak correlation is slightly higher (0.28) at zero lag. A secondary peak at a 6-day lag is not significant. A more pronounced peak of 0.50 at a one day lag for station 5 is seen. But given the lower correlations at stations 3 and 4, this most likely reflects coherent large-scale forcing rather than wave propagation.

The results are consistent with the current meter analysis of LaCasce (2005), which suggested short correlation scales ($L < 15$ km) in the across-slope velocity along the slope. Using a model with 4-km resolution, LaCasce and Engedahl (2005) observed significant correlations at longer separations than indicated by the current meters, suggesting wave transmission was improved with the smoothed bathymetry. But the correlations were nevertheless insignificant for separations exceeding 50 km.

4. Discussion

a. *Drivers of short-term variability*

In terms of the candidates for drivers of current variability described in the introduction, the correspondence we see

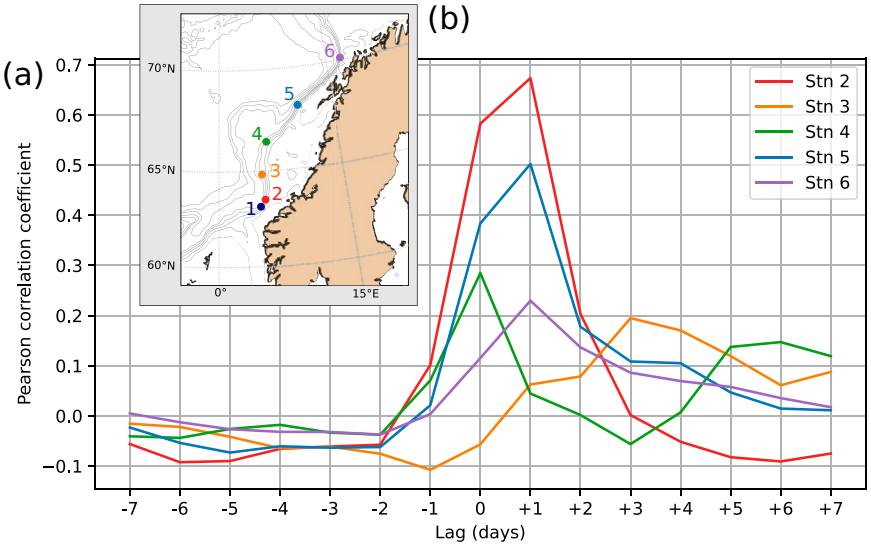

FIG. 10. (a) Lagged correlations between across-slope velocities from TOPAZ4 at a depth of 763 m, at each of locations 2–6 shown in (b) and at location 1. A positive lag indicates comparison with a later date at the more northerly location.

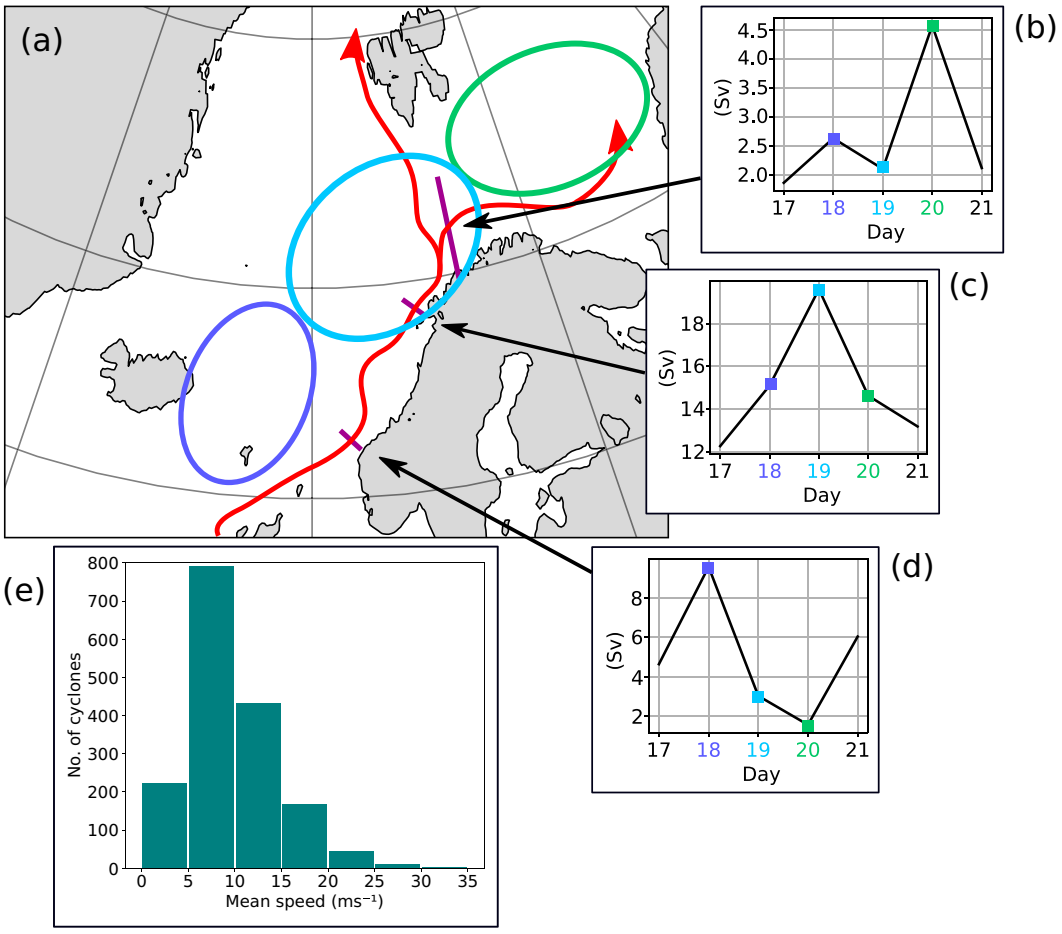

FIG. 11. (a) Example of a cyclone moving through the Nordic and Barents Seas. The blue, turquoise, and green ovals mark the positions of the cyclone center, as indicated by ERA-Interim daily mean SLP data, on 18, 19, and 20 December 1992. The red line shows the main path of the NwASC. (b)–(d) Volumetric transports across the transects at BSO, Gimsøy, and Svinøy respectively [shown by the purple lines in (a)] for the period from 17 to 21 December 1992, as calculated from TOPAZ4 ocean velocities. (e) Mean speeds of cyclones in ERA-Interim within the Nordic seas region (60°–75°N, 15°W–35°E), during the months NDJFM in the period 1990–2018.

between local atmospheric conditions and ocean currents is consistent with candidate 2, local wind forcing. If covariability is seen between flows at different locations along the path of the current, this might instead suggest a role for candidate 1, shelf waves initiated by remote atmospheric forcing upstream of the study locations. And we do indeed see (Fig. 9) a relatively high lagged correlation between Svinøy and Gimsøy, which would be consistent with a shelf wave propagating at a speed of around 1250 km in 24 h, or approximately 15 m s^{-1}. [Drivdal et al. (2016) estimated shelf wave propagation speeds along the coast here to lie within the range 5–24 m s^{-1}.] But no evidence for these is apparent in our analysis of across-slope velocities. Instead, we offer an alternative, simpler, explanation for the covariance, an explanation that is consistent with local wind forcing. It so happens that the cyclones that give rise to peaks in flow also tend to track up the coast at a similar speed, and so any lags seen in the correlation maxima can be understood simply as the result of the weather systems providing local wind forcing at each location in succession as they move, without any need to invoke shelf waves to carry a signal of the forcing. An illustration of this effect is given in Fig. 11, which shows the successive positions, about 1000 km apart, of a single cyclone on 18, 19, and 20 December 1992 and the consequent peaks in ocean current successively at Svinøy, Gimsøy, and BSO over the same period as it passes each location. The propagation speed of the cyclone in this example is approximately 13 m s^{-1}. Figure 11e shows the mean speeds of all winter [November–March (NDJFM)] cyclones within the Nordic seas region. The bulk of these are between 5 and 25 m s^{-1}, which by coincidence matches closely the typical wave propagation speeds given by Drivdal et al. (2016).

This is not to say that we dismiss coastally trapped waves as a mechanism for propagating a signal of variability. They have been found to be important on the northern and southern American continental shelves (Brink 1991), but there is

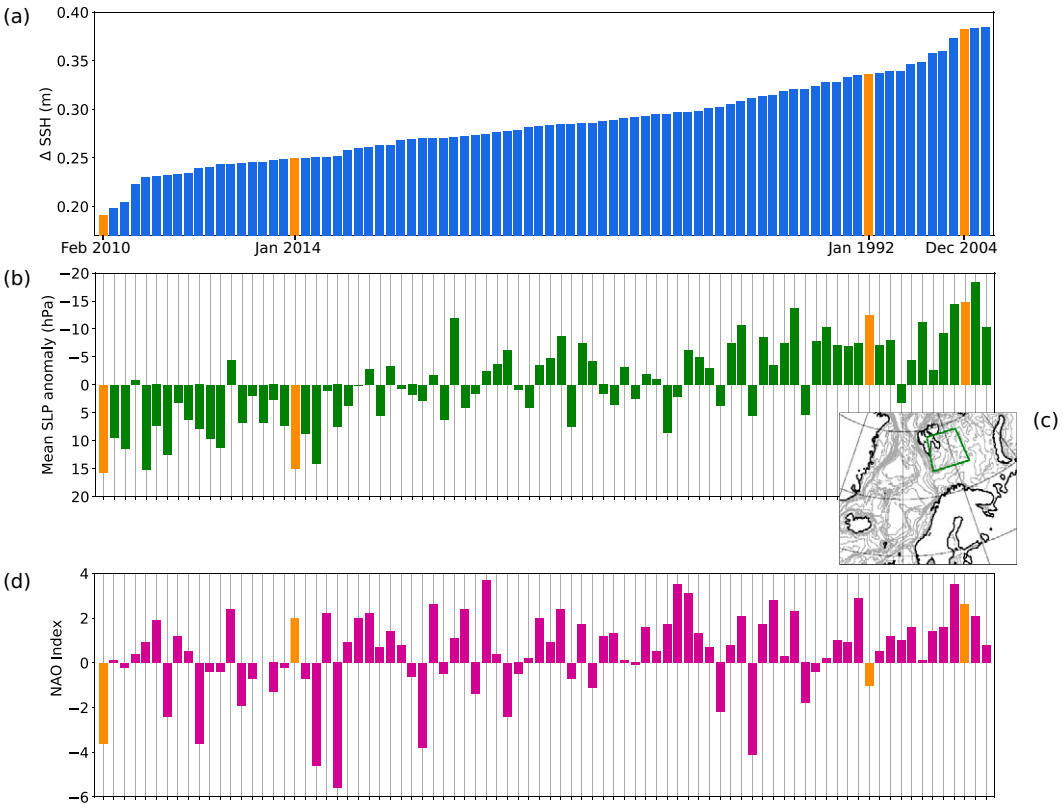

FIG. 12. (a) Monthly mean gradient in TOPAZ SSH along the BSO transect, for winter (DJF) months ordered from low gradient to high gradient. (b) Monthly mean SLP anomalies from ERA-Interim, averaged over the area outlined in green in (c), for the same ordered list of months. (Note the reversed *y* axis.) (d) Monthly mean Hurrell North Atlantic Oscillation (NAO) station-based index for the ordered list of months. Orange bars indicate the months for which SLP anomalies are shown in Fig. 13.

conflicting evidence for their existence along the Norwegian coast. Idealized numerical simulations of the ocean response to low pressure systems traveling along the Norwegian coast have indicated their presence, both in the form of Kelvin waves and continental shelf waves (Martinsen et al. 1979; Drivdal et al. 2016). On the other hand, LaCasce (2005) failed to find evidence for them in current meter data here. We suggest that the reason these studies have reached different conclusions lies in the location of the Nordic seas on the main storm track for cyclones generated over the North Atlantic. Shelf waves probably do exist here, but they are masked by the stronger direct forcing from passing cyclones, and so any coherent propagating signal would be difficult to observe in realistic data.

A further cause of the spatial incoherence that LaCasce (2005) found in velocity fluctuations over the slope could be the small-scale eddies resulting from instabilities in the current (candidate 3 in section 1). These cannot explain extreme flow events—which are larger-scale coherent responses—but probably contribute to the noise in the current time series.

To summarize, our findings support those of Ingvaldsen et al. (2004), who related variability in the velocity field at the inflow to the Barents Sea to sea level changes arising from Ekman transport, and Richter et al. (2009), who linked variability in the inflow to the Nordic seas to local atmospheric forcing. They are also consistent with the locally forced leading EOF mode that Skagseth and Orvik (2002) found in mooring measurements from Svinøy. Those authors identified a roughly 12-h delay in the ocean response relative to the forcing; we cannot resolve such a short time scale since we use daily means for both ocean velocities and atmospheric pressure, but it would be reasonable to expect sea surface heights to evolve over the inertial time scale governing Ekman transport, which is also around 12 h at these latitudes.

b. *Implications for longer time scales*

The daily resolution of the model data we have used does, however, allow us to revisit the findings of earlier studies of coherence of the NwASC at longer time scales. On monthly time scales, Skagseth (2004) found coherent along-stream variability at zero lag ($r = 0.70$) along the entire NwASC in a study using satellite altimetry data. They concluded that their results were consistent with a direct response of the current to the large-scale wind field. But monthly time scales are long compared to the time taken for the passage of individual weather systems over the Nordic seas. Over these time scales,

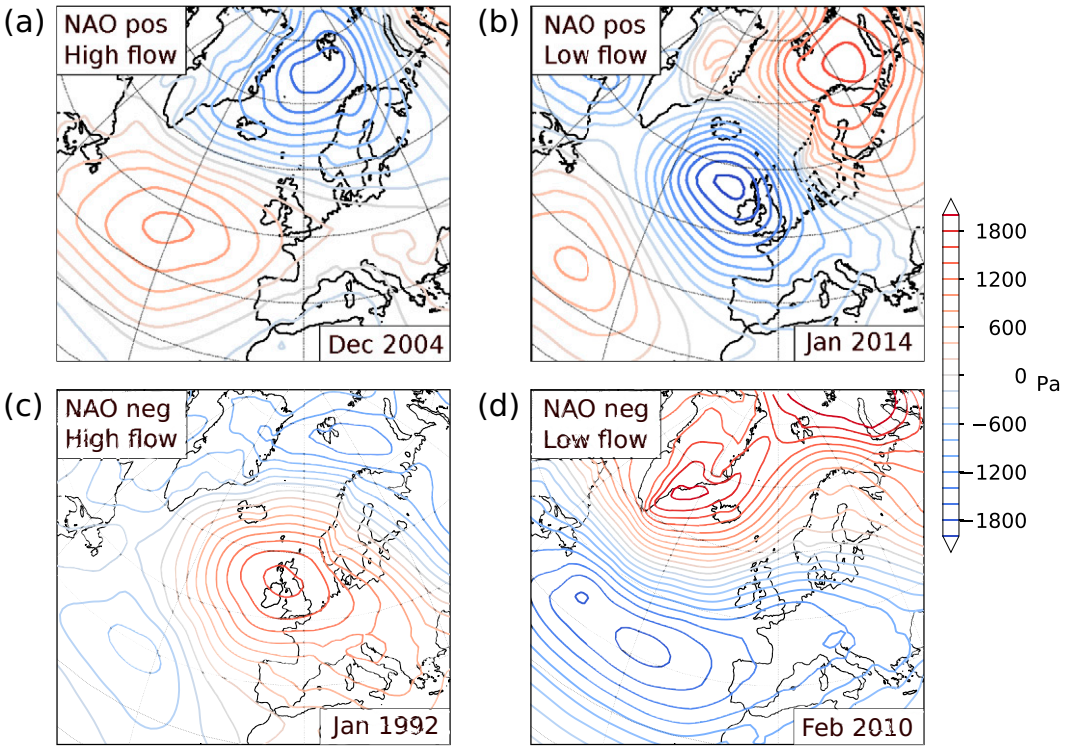

FIG. 13. Monthly mean anomalies in SLP for (a) December 2004, (b) January 2014, (c) January 1992, and (d) February 2010.

all locations along the path of the current "see" similar wind forcing, and the ocean response appears simultaneous at all locations. Analysis of the current using model data instead allows us to identify the ocean response to forcing more precisely in time, and thus in space, revealing the lags in correlation peaks as weather systems move along the path of the current and pointing to local winds, rather than large-scale forcing, as the main driver of variability.

Over even longer time scales, Calafat et al. (2013) found coherent sea level fluctuations along the Norwegian and part of the Arctic coast. They attributed these partly to regional wind forcing, but partly to the propagation of a signal generated farther south, on the eastern boundary of the North Atlantic. Our analysis of short-term variability in the shelf current has not identified a mechanism that could explain such a connection.

Chafik et al. (2015) proposed direct local (they used the term "regional") atmospheric forcing as the main driver for the variability they saw over monthly and longer time scales in what they term the Fram Strait branch of the current, which flows across our Sørkapp transect and northward along the west coast of Spitsbergen. What is the mechanistic explanation for this relationship, when the weather systems are associated with much shorter time scales? In Fig. 12a we show—as an aggregate indicator of flow strength—monthly means of difference in SSH along the BSO. (We show this transect here, rather than Sørkapp, for clarity, because we have found that individual extreme events at Sørkapp are associated with a greater variety of atmospheric conditions than those at BSO, but we argue that the principle applies generally.) As we wish to compare this to an index of the passing of strong cyclones, we have plotted in Fig. 12b the average SLP in a limited region in the Barents Sea north of the BSO line (see geographical insert in Fig. 12c). This index is chosen to reflect both the number of cyclones passing through the locality and their strength. The months have been ordered from left to right according to mean difference in SSH. In broad terms (Pearson correlation coefficient = −0.76), we see that low mean atmospheric pressure, an indicator of more and/or stronger cyclones, is associated with higher flows, and vice versa for higher SLP and lower flows. We conclude, therefore, that the link between local wind forcing and ocean transports does hold over time scales of a month because the longer-term behavior of the ocean is simply an integration over higher-frequency signals.

c. *North Atlantic Oscillation*

Other previous studies [see Furevik and Nilsen (2005) for a summary] have linked variability in the NwAC, especially at Svinøy, to large-scale atmospheric forcing, as characterized by the NAO index. In Fig. 12d we also show the Hurrell NAO index for each sorted month. The correlation between the NAO index and the monthly mean flow at BSO is much less (correlation coefficient = 0.33) than the correlation with the SLP locally in the Barents Sea (0.76). That variability in flow into the Barents Sea should be more closely related to SLP in the locality than to the NAO is unsurprising. (Of course, it is

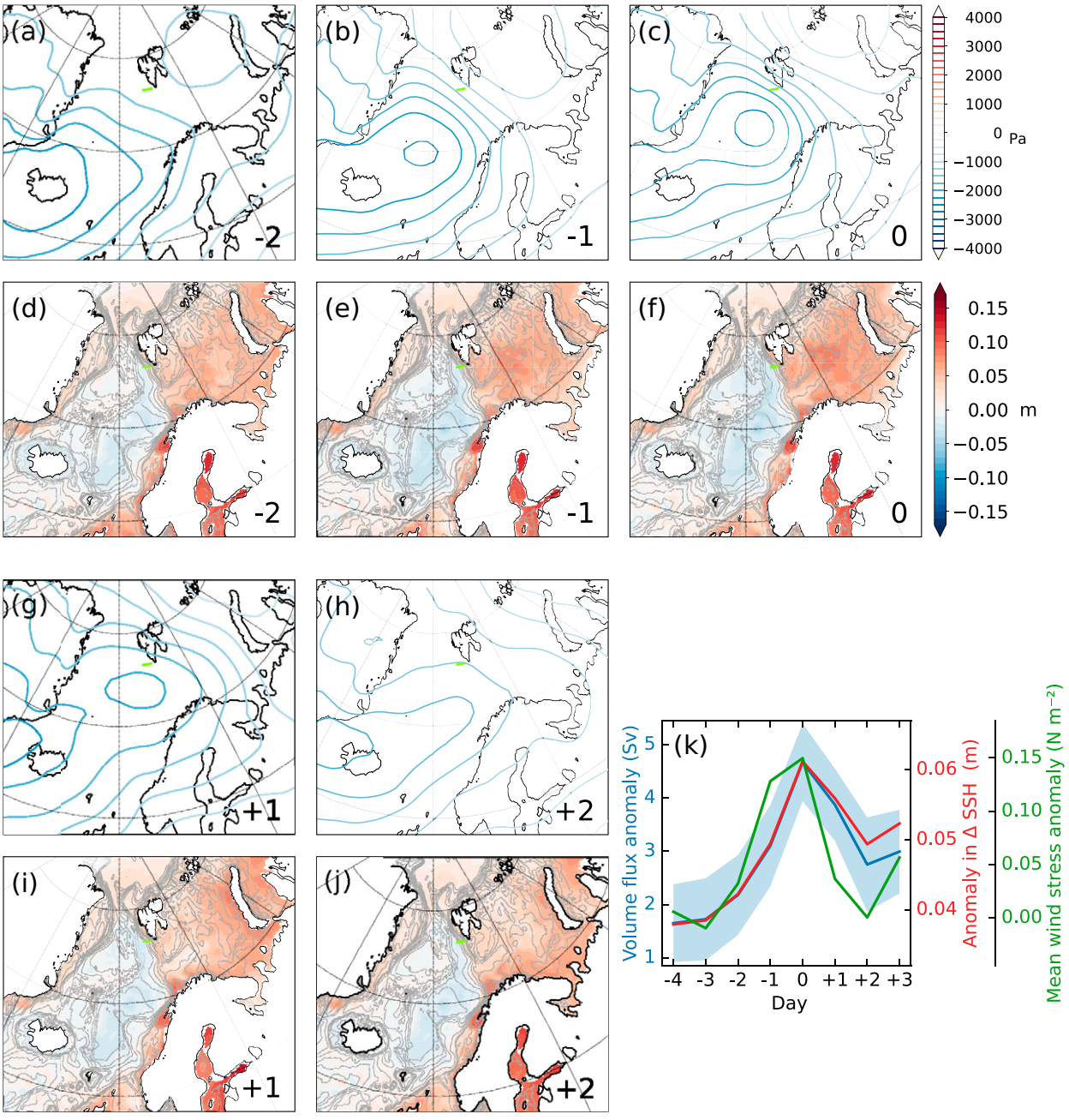

FIG. A1. (a) Mean anomalies in SLP from ERA-Interim for all dates two days before the first day of each high flow event at Sørkapp (day −2). (b),(c),(g),(h) The same, but for days −1, 0, +1, and +2, respectively. (d)–(f) (i),(j) Mean anomalies in TOPAZ SSH for the same groups of days. (k) Mean anomalies in volumetric transport (blue), SSH difference (red), and along-slope wind stress (green) at Sørkapp for all dates from four days before to three days after the first days of extreme flow events. The blue shading indicates standard error (±1 standard deviation divided by $\sqrt{N}$) in volumetric transport for days included in the composite.

gradient in SLP that drives winds; here we are using SLP as a proxy for the SLP gradient associated with cyclones.) The NAO index is an indicator of a large-scale atmospheric state: the meridional pressure differential in the North Atlantic. As a rule, positive values are associated with increased cyclone activity along the main storm track northeastward into the Nordic seas. But the paths taken by individual cyclones can vary quite considerably, and as we have seen from Figs. 5, 7, 8, and A1 the effect of a cyclone on the variability of flow in each branch of the NwAC depends on the particular route it takes. More generally, large-scale atmospheric patterns that give rise to positive NAO values may nevertheless incorporate quite different features at the regional level. See Chafik et al. (2017) for an account of the interaction between the

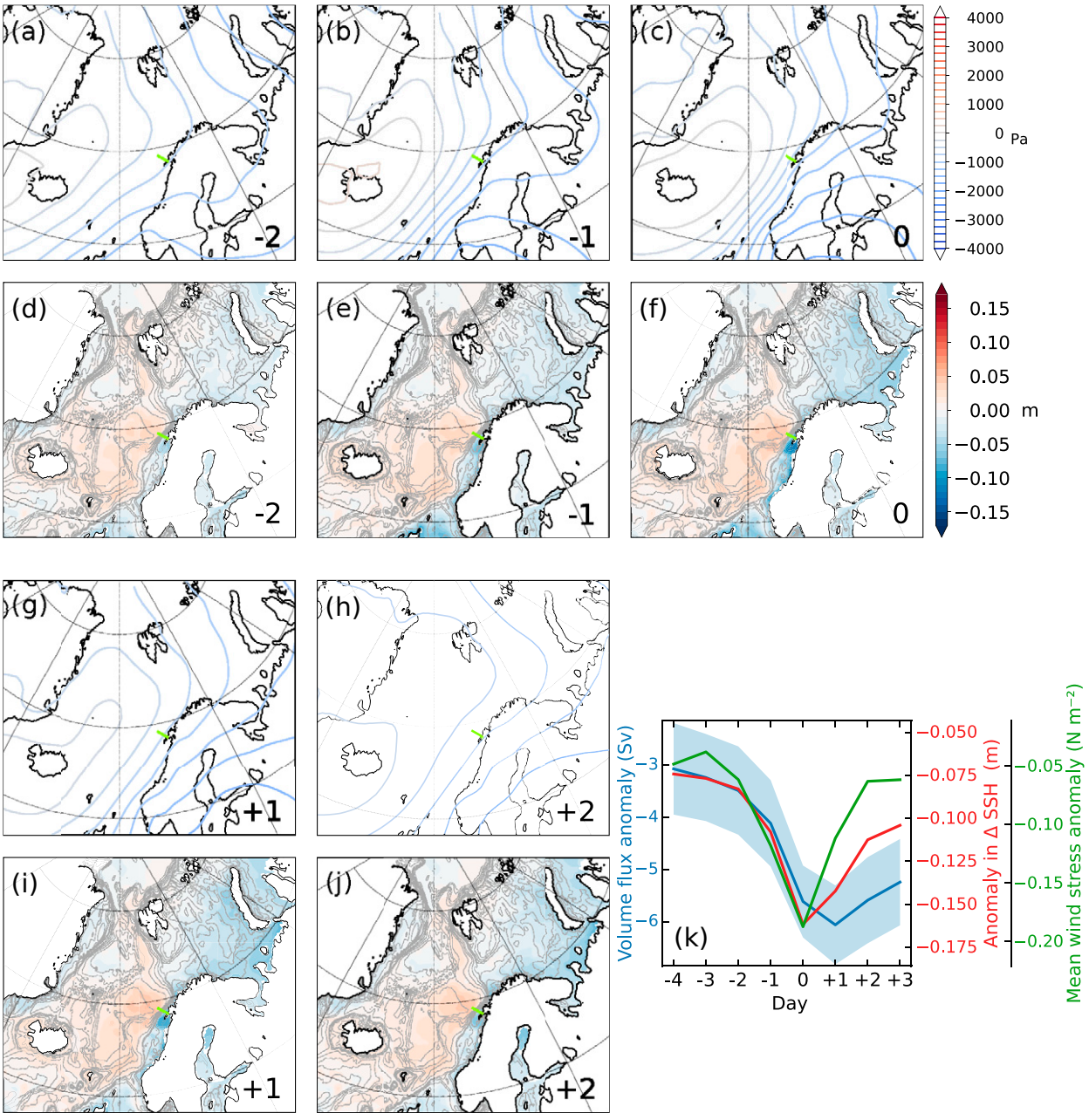

FIG. A2. As Fig. A1, but for low flow events at Gimsøy.

NAO and other telecommunication patterns, and its influence on sea level on the northern European shelf. To illustrate this last point we show anomalies in monthly mean SLP for four contrasting months in Fig. 13. (The months are shown in orange in Fig. 12.) In both December 2004 (Fig. 13a) and January 2014 (Fig. 13b), the NAO index was positive (2.6 and 2.0, respectively), but the centers of the pressure anomalies are shifted markedly from one to the other. In December 2004 a negative pressure anomaly centered over Spitsbergen led to stronger than average winds and a strengthened current into the Barents Sea, while in January 2014 a positive SLP anomaly over the Barents Sea retarded the Barents Sea inflow. Likewise, negative NAO conditions were experienced in both January 1992 (Fig. 13c; −1.0) and February 2010 (Fig. 13d; −1.9), but the former case saw winds and current strengthened into the Barents Sea, while in the latter the reverse was true.

d. *Other weather regimes*

In recent years there has been a growing interest in weather regimes in general. These are quasi-stationary states such as blocking systems, caused by fluctuations in the jet stream at

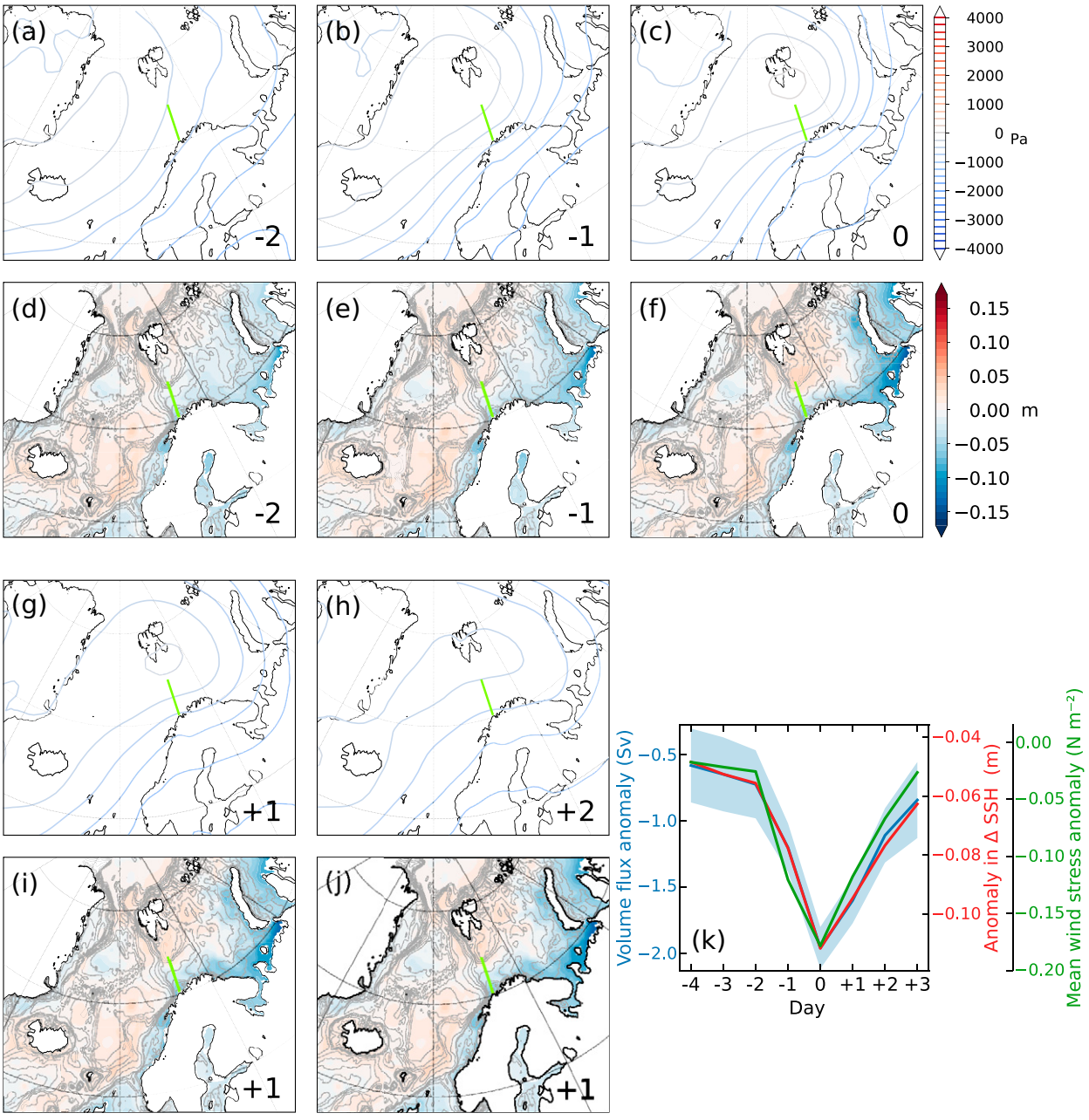

FIG. A3. As Fig. A1, but for low flow events at BSO.

midlatitudes. Madonna et al. (2017) showed that the atmosphere over the North Atlantic preferentially occupies one of five dominant weather regimes, which better capture spatial configurations of the jet stream than do simple indices such as the NAO. Barrier et al. (2013) studied the response of the subtropical North Atlantic Ocean to similar patterns of atmospheric forcing. Their conclusion was that the ocean in this region is not equally sensitive to all regimes. A strong response was seen only in the case of the regime termed the "Atlantic Ridge." Under that regime, anticyclonic wind anomalies form off Europe and the climatological wind stress curl is shifted northward, leading to a strengthening of the subtropical gyre. Weather regime definitions that partition variability based directly on the atmospheric flow have also been shown to influence sea level around the northern European continental shelf (Mangini et al. 2021). In our study, we found that daily variability in the NwASC is related to the five North Atlantic weather regimes only insofar as they tend to give rise to along-slope winds in the Nordic seas. Instead we have shown that this far north, local wind conditions related to the passing

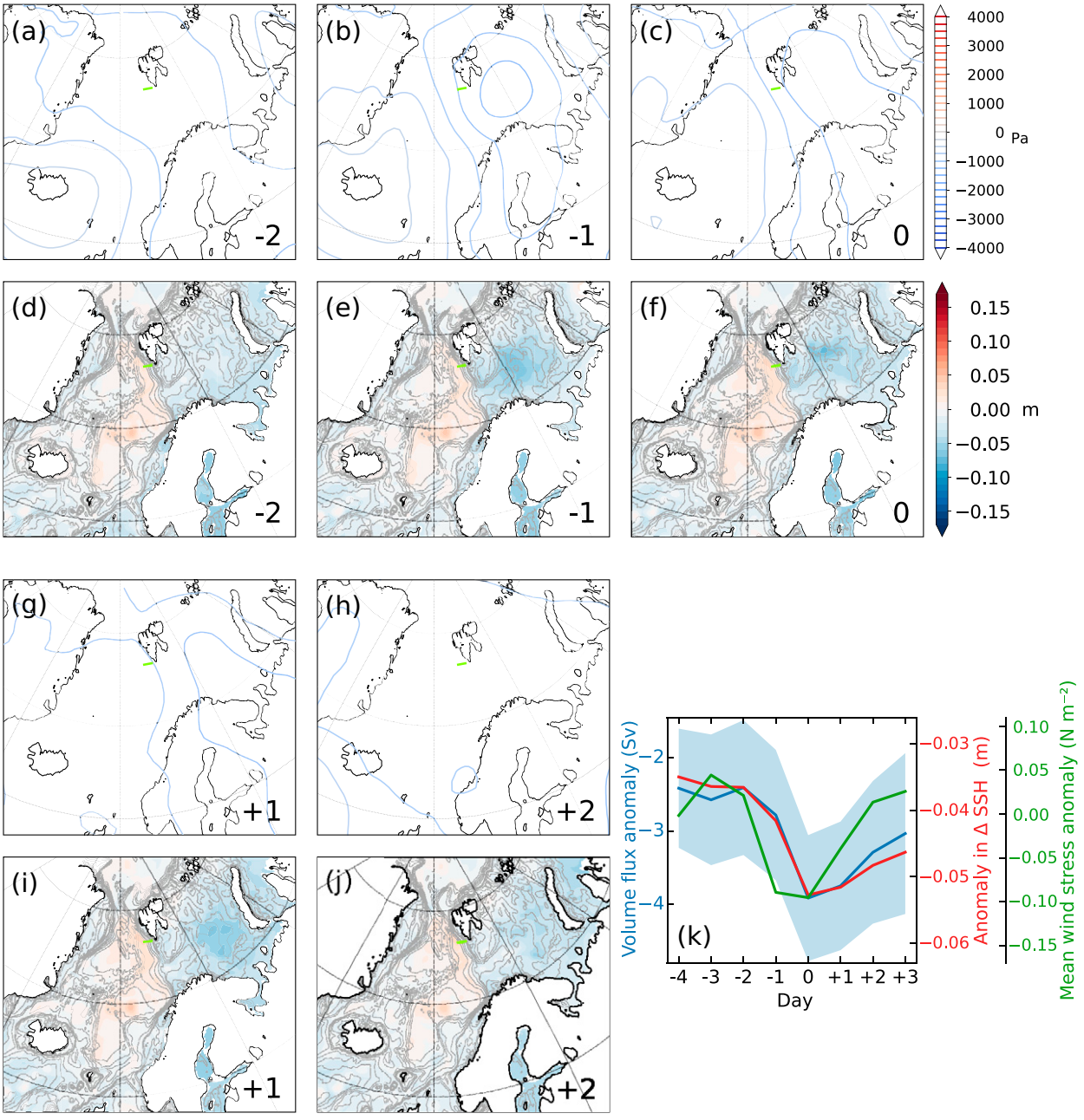

FIG. A4. As Fig. A1, but for low flow events at Sørkapp.

of cyclones and anticyclones through the Nordic seas rather than to quasi-stationary midlatitude dynamics are the primary cause of variability in the current.

5. Summary

We have used 28 years' worth of satellite altimetry and ocean reanalysis data for the Nordic seas and Barents Sea to explore the drivers of short-term variability in the main current flowing along the Norwegian slope toward the Arctic Ocean. We have aimed to distinguish between three potential candidates: that the variability is associated with shelf waves triggered by remote atmospheric disturbances which propagate along the Norwegian shelf, the path of the current; that it is caused by direct, local atmospheric forcing; or that it is caused by eddies generated by instabilities in the current.

We have found a close relationship between strong flow anomalies along the NwASC and the local wind field, indicating that over time scales of a few days local atmospheric forcing is the main driver. Ekman transport associated with the wind field of passing cyclones leads to a piling up of water on the Norwegian shelf over inertial time scales, with the

resultant increase in horizontal pressure gradient yielding an increase in the geostrophic shelf current. Topographic PV gradients constrain the pressure and geostrophic flow anomalies to essentially line up with the continental slope below. In the reverse process, Ekman transport during periods of high atmospheric pressure over the central basins draws water off the shelf, leading to a slowing or occasional reversal of the current.

Our results do not indicate that remote atmospheric forcing has a strong effect. A lag of a day or so in the covariability of the current at locations along its path, which would be consistent with the expected phase propagation speed of a shelf wave, can be explained instead by the passage of weather systems along the same path, which causes direct wind forcing sequentially at each location.

Intrinsic ocean variability, caused by mesoscale and submesoscale baroclinic and shear instability, will also add variability in the current. But such variability is obviously incoherent over the large spatial scales observed in this work and can primarily be expected to be responsible for some of the spread, or noise, in our estimates. Note, too, that the eddies generated by instabilities will be more important to variability at a point location, and will to some extent be integrated out when transports are integrated over a longer section, as we have done here.

Finally, we have seen indications that the short-time atmospheric forcing can be integrated in time to make net effects on monthly time scales. Specifically, the flow into the Barents Sea behaves simply as an integration of short-term responses to short-term forcing events. The NAO index, as an index of large-scale atmospheric variability, is not correlated well with current variability in this region because the large-scale atmospheric states that it describes encompass a variety of features at the regional and local scale here, only some of which give rise to a strong ocean response.

Acknowledgments. This work was funded by the Research Council of Norway through the project The Nansen Legacy (RCN 276730). JHL also acknowledges the support of the Research Council of Norway through the Rough Ocean project (RCN 302743). The authors are grateful for the thoughtful comments from two anonymous reviewers, which greatly strengthened the paper.

Data availability statement. The SSALTO/DUACS delayed-time multi-satellite product is distributed by the European Copernicus Marine Environment Monitoring Service (CMEMS; https://resources.marine.copernicus.eu/?option=com_csw&view=details&product_id=SEALEVEL_GLO_PHY_L4_REP_OBSERVATIONS_008_047), and MDT is at https://resources.marine.copernicus.eu/product-detail/SEALEVEL_GLO_PHY_MDT_008_063/DATA-ACCESS. TOPAZ4 reanalysis data are available from CMEMS at https://data.marine.copernicus.eu/product/ARCTIC_MULTIYEAR_PHY_002_003/description. ERA-Interim data can be downloaded from the portal of the European Centre for Medium-Range Weather Forecasts (ECMWF; https://www.ecmwf.int/en/forecasts/datasets/reanalysis-datasets/era-interim).

APPENDIX

Ocean Response to Atmospheric Forcing: Further Examples

Figures A1–A4 show the development of sea level anomalies and associated atmospheric pressure anomalies for extreme-flow situations opposite to those shown in Figs. 5–8.

REFERENCES

Adams, J. K., and V. T. Buchwald, 1969: The generation of continental shelf waves. *J. Fluid Mech.*, **35**, 815–826, https://doi.org/10.1017/S0022112069001455.

Allen, J. S., 1975: Coastal trapped waves in a stratified ocean. *J. Phys. Oceanogr.*, **5**, 300–325, https://doi.org/10.1175/1520-0485(1975)005<0300:CTWIAS>2.0.CO;2.

Barrier, N., A.-M. Treguier, C. Cassou, and J. Deshayes, 2013: Impact of the winter North-Atlantic weather regimes on subtropical sea-surface height variability. *Climate Dyn.*, **41**, 1159–1171, https://doi.org/10.1007/s00382-012-1578-7.

Brink, J. H., 1991: Coastal-trapped waves and wind-driven currents over the continental shelf. *Ann. Rev. Fluid Dyn.*, **23**, 389–412, https://doi.org/10.1146/annurev.fl.23.010191.002133.

Calafat, F. M., D. P. Chambers, and M. N. Tsimplis, 2013: Interannual to decadal sea-level variability in the coastal zones of the Norwegian and Siberian Seas: The role of atmospheric forcing. *J. Geophys. Res. Oceans*, **118**, 1287–1301, https://doi.org/10.1002/jgrc.20106.

Chafik, L., J. Nilsson, Ø. Skagseth, and P. Lundberg, 2015: On the flow of Atlantic water and temperature anomalies in the Nordic Seas toward the Arctic Ocean. *J. Geophys. Res. Oceans*, **120**, 7897–7918, https://doi.org/10.1002/2015JC011012.

——, J. E. Ø. Nilsen, and S. Dangendorf, 2017: Impact of North Atlantic teleconnection patterns on Northern European sea level. *J. Mar. Sci. Eng.*, **5**, 43, https://doi.org/10.3390/jmse5030043.

Dee, D. P., and Coauthors, 2011: The ERA-Interim reanalysis: Configuration and performance of the data assimilation system. *Quart. J. Roy. Meteor. Soc.*, **137**, 553–597, https://doi.org/10.1002/qj.828.

Drivdal, M., J. E. H. Weber, and J. B. Debernard, 2016: Dispersion relation for continental shelf waves when the shallow shelf part has an arbitrary width: Application to the shelf west of Norway. *J. Phys. Oceanogr.*, **46**, 537–549, https://doi.org/10.1175/JPO-D-15-0023.1.

Fer, I., A. Bosse, and J. Dugstad, 2020: Norwegian Atlantic slope current along the Lofoten Escarpment. *Ocean Sci.*, **16**, 685–701, https://doi.org/10.5194/os-16-685-2020.

Furevik, T., and J. E. Ø. Nilsen, 2005: Large-scale atmospheric circulation variability and its impacts on the Nordic Seas ocean climate: A review. *The Nordic Seas: An Integrated perspective, Geophys. Monogr.*, Vol. 158, Amer. Geophys. Union, 105–136, https://doi.org/10.1029/158GM09.

Gill, A. E., and E. H. Schumann, 1974: The generation of long shelf waves by the wind. *J. Phys. Oceanogr.*, **4**, 83–90, https://doi.org/10.1175/1520-0485(1974)004<0083:TGOLSW>2.0.CO;2.

Gordon, R. L., and J. M. Huthnance, 1987: Storm-driven continental shelf waves over the Scottish continental shelf. *Cont. Shelf Res.*, **7**, 1015–1048, https://doi.org/10.1016/0278-4343(87)90097-5.

Hakim, G. J., C. Snyder, and D. J. Muraki, 2002: A new surface model for cyclone–Anticyclone asymmetry. *J. Atmos. Sci.*, **59**, 2405–2420, https://doi.org/10.1175/1520-0469(2002)059<2405:ANSMFC>2.0.CO;2.

Ingvaldsen, R. B., L. Asplin, and H. Loeng, 2004: Velocity field of the western entrance to the Barents Sea. *J. Geophys. Res.*, **109**, C03021, https://doi.org/10.1029/2003JC001811.

Isachsen, P. E., J. H. LaCasce, C. Mauritzen, and S. Häkkinen, 2003: Wind-driven variability of the large-scale recirculating flow in the Nordic seas and Arctic Ocean. *J. Phys. Oceanogr.*, **33**, 2534–2550, https://doi.org/10.1175/1520-0485(2003)033<2534:WVOTLR>2.0.CO;2.

——, I. Koszalka, and J. H. LaCasce, 2012: Observed and modeled surface eddy heat fluxes in the eastern Nordic Seas. *J. Geophys. Res.*, **117**, C08020, https://doi.org/10.1029/2012JC007935.

LaCasce, J. H., 2005: Statistics of low frequency currents over the western Norwegian shelf and slope I: Current meters. *Ocean Dyn.*, **55**, 213–221, https://doi.org/10.1007/s10236-005-0021-6.

——, and H. Engedahl, 2005: Statistics of low frequency currents over the western Norwegian shelf and slope II: Model. *Ocean Dyn.*, **55**, 222–237, https://doi.org/10.1007/s10236-005-0022-5.

Lien, V. S., F. B. Vikebø, and Ø. Skagseth, 2013: One mechanism contributing to co-variability of the Atlantic inflow branches to the Arctic. *Nat. Commun.*, **4**, 1488, https://doi.org/10.1038/ncomms2505.

Madonna, E., C. Li, C. M. Grams, and T. Woollings, 2017: The link between eddy-driven jet variability and weather regimes in the North Atlantic-European sector. *Quart. J. Roy. Meteor. Soc.*, **143**, 2960–2972, https://doi.org/10.1002/qj.3155.

Mangini, F., L. Chafik, E. Madonna, C. Li, L. Bertino, and J. E. Ø. Nilsen, 2021: The relationship between the eddy-driven jet stream and northern European sea level variability. *Tellus*, **73A**, 1886419, https://doi.org/10.1080/16000870.2021.1886419.

Martinsen, E. A., B. Gjevik, and L. P. Röed, 1979: A numerical model for long barotropic waves and storm surge along the western coast of Norway. *J. Phys. Oceanogr.*, **9**, 1126–1138, https://doi.org/10.1175/1520-0485(1979)009<1126:ANMFLB>2.0.CO;2.

Mulet, S., and Coauthors, 2021: The new CNES-CLS18 global mean dynamic topography. *Ocean Sci.*, **17**, 789–808, https://doi.org/10.5194/os-17-789-2021.

Nøst, O. A., and P. E. Isachsen, 2003: The large-scale time-mean ocean circulation in the Nordic Seas and Arctic Ocean estimated from simplified dynamics. *J. Mar. Res.*, **61**, 175–210, https://doi.org/10.1357/002224003322005069.

Oke, P., and Coauthors, 2015: Assessing the impact of observations on ocean forecasts and reanalyses: Part 1, Global studies. *J. Oper. Oceanogr.*, **8**, s49–s62, https://doi.org/10.1080/1755876X.2015.1022067.

Orvik, K. A., 2022: Long-term moored current and temperature measurements of the Atlantic inflow into the Nordic Seas in the Norwegian Atlantic Current: 1995–2020. *Geophys. Res. Lett.*, **49**, e2021GL096427, https://doi.org/10.1029/2021GL096427.

——, and P. Niiler, 2002: Major pathways of Atlantic water in the northern North Atlantic and Nordic Seas toward Arctic. *Geophys. Res. Lett.*, **29**, 1896, https://doi.org/10.1029/2002GL015002.

——, and Ø. Skagseth, 2003a: The impact of the wind stress curl in the North Atlantic on the Atlantic inflow to the Norwegian Sea toward the Arctic. *Geophys. Res. Lett.*, **30**, 1884, https://doi.org/10.1029/2003GL017932.

——, and ——, 2003b: Monitoring the Norwegian Atlantic slope current using a single moored current meter. *Cont. Shelf Res.*, **23**, 159–176, https://doi.org/10.1016/S0278-4343(02)00172-3.

Poulain, P.-M., A. Warn-Varnas, and P. P. Niiler, 1996: Near-surface circulation of the Nordic seas as measured by Lagrangian drifters. *J. Geophys. Res.*, **101**, 18 237–18 258, https://doi.org/10.1029/96JC00506.

Pujol, M.-I., Y. Faugère, G. Taburet, S. Dupuy, C. Pelloquin, M. Ablain, and N. Picot, 2016: DUACS DT2014: The new multi-mission altimeter data set reprocessed over 20 years. *Ocean Sci.*, **12**, 1067–1090, https://doi.org/10.5194/os-12-1067-2016.

——, P. Schaeffer, Y. Faugère, M. Raynal, G. Dibarboure, and N. Picot, 2018: Gauging the improvement of recent mean sea surface models: A new approach for identifying and quantifying their errors. *J. Geophys. Res. Oceans*, **123**, 5889–5911, https://doi.org/10.1029/2017JC013503.

Richter, K., T. Furevik, and K. A. Orvik, 2009: Effect of wintertime low-pressure systems on the Atlantic inflow to the Nordic seas. *J. Geophys. Res.*, **114**, C09006, https://doi.org/10.1029/2009JC005392.

——, O. H. Segtnan, and T. Furevik, 2012: Variability of the Atlantic inflow to the Nordic Seas and its causes inferred from observations of sea surface height. *J. Geophys. Res.*, **117**, C04004, https://doi.org/10.1029/2011JC007719.

Sakov, P., F. Counillon, L. Bertino, K. A. Lisæter, P. R. Oke, and A. Korablev, 2012: TOPAZ4: An ocean-sea ice data assimilation system for the North Atlantic and Arctic. *Ocean Sci.*, **8**, 633–656, https://doi.org/10.5194/os-8-633-2012.

Skagseth, Ø., 2004: Monthly to annual variability of the Norwegian Atlantic slope current: Connection between the northern North Atlantic and the Norwegian Sea. *Deep-Sea Res. I*, **51**, 349–366, https://doi.org/10.1016/j.dsr.2003.10.014.

——, and K. A. Orvik, 2002: Identifying fluctuations in the Norwegian Atlantic Slope Current by means of empirical orthogonal functions. *Cont. Shelf Res.*, **22**, 547–563, https://doi.org/10.1016/S0278-4343(01)00086-3.

Thorpe, A. J., 1986: Synoptic scale disturbances with circular symmetry. *Mon. Wea. Rev.*, **114**, 1384–1389, https://doi.org/10.1175/1520-0493(1986)114<1384:SSDWCS>2.0.CO;2.

Timmermans, M.-L., and J. Marshall, 2020: Understanding Arctic Ocean circulation: A review of ocean dynamics in a changing climate. *J. Geophys. Res. Oceans*, **125**, e2018JC014378, https://doi.org/10.1029/2018JC014378.

Trodahl, M., and P. E. Isachsen, 2018: Topographic influence on baroclinic instability and the mesoscale eddy field in the northern North Atlantic Ocean and the Nordic Seas. *J. Phys. Oceanogr.*, **48**, 2593–2607, https://doi.org/10.1175/JPO-D-17-0220.1.

Volkov, D. L., and M.-I. Pujol, 2012: Quality assessment of a satellite altimetry data product in the Nordic, Barents, and Kara Seas. *J. Geophys. Res.*, **117**, C03025, https://doi.org/10.1029/2011JC007557.

Xie, J., L. Bertino, F. Counillon, K. A. Lisæter, and P. Sakov, 2017: Quality assessment of the TOPAZ4 reanalysis in the Arctic over the period 1991–2013. *Ocean Sci.*, **13**, 123–144, https://doi.org/10.5194/os-13-123-2017.